Effect of shape in near-field thermal transfer for periodic structures

Hamidreza Chalabi,[1,*] Erez Hasman,[2,†] and Mark L. Brongersma[1,‡]
[1]*Geballe Laboratory for Advanced Materials, Stanford University, Stanford, California 94305, USA*
[2]*Micro and Nanooptics Laboratory, Faculty of Mechanical Engineering, and Russell Berrie Nanotechnology Institute, Technion-Israel Institute of Technology, Haifa 32000, Israel*
(Received 24 March 2015; revised manuscript received 6 May 2015; published 26 May 2015)

In this paper, the effect of the geometrical shape on the radiative thermal transfer between a periodic array of beams and a planar substrate is investigated. Specifically, we analyze the changes in the thermal transfer that occur when the cross-sectional shape of SiC beams is modified from rectangular to ellipsoidal and finally triangular. Numerical calculations are done based on the rigorous coupled wave analysis. These exact results from this analysis are compared to modified proximity and far-field approximations, which become valid for small and large spacings, respectively. Moreover, these results are also compared to effective medium theory, which becomes increasingly accurate in the limit of small periodicities. We show that a reduction in the periodicity will lead to a reduced thermal transfer for triangular and ellipsoidal shaped beams. Even though, in the limit of very small periodicity, thermal transfer for the case of rectangular shaped beams also decreases by decreasing the periodicity, this decrease is slower as compared to other cross-sectional shapes. Finally, we show that even though changing periodicity will change the magnitude of thermal transfer, the scaling law for its variation with the beam to substrate spacing is primarily determined by the cross-sectional shape rather than the periodicity. We analytically prove this fact by investigating the large and small periodicity regimes.

DOI: 10.1103/PhysRevB.91.174304 PACS number(s): 44.05.+e, 44.40.+a, 05.40.−a

I. INTRODUCTION

Near-field thermal transfer [1–3] between two bodies shows a dramatic enhancement over the far-field radiative thermal transfer which obeys Planck's law [4]. This fact has inspired researchers to generate similar techniques for controlling the near-field thermal transfer similar to the ones that have been developed for controlling thermal emission [5–8]. Such efforts have led to the design of nanostructures for a variety of applications such as thermal rectifiers [9], thermal diodes [10], and near-field thermal transistors [11].

In order to control near-field thermal transfer, use has been made of structures with subwavelength features. In spite of a myriad of available optical software packages, finding numerical solutions for near-field thermal transfer can be challenging and requires tremendous computational power for even very simple geometries. As a result, there have been intense efforts to develop new, efficient numerical techniques that enable calculation of thermal transfer for specific geometries. Geometries that are considered range from planar structures [1,12,13] to cases where a sphere [14–16], a cone [16], or a cylinder [16] is placed on top of a planar substrate. There are several reviews that summarize the results of this line of research [17,18]. In addition to a variety of exact numerical techniques, there also exists a set of approximation methods for thermal transfer calculations. Among them, the most popular are the effective medium theory that is used for subwavelength periodic structures [19–24], the proximity approximation and its modified version [25–27], and the coupled mode theory [9,28,29].

In this paper we use the method developed in Ref. [27] to investigate the impact of the cross-sectional shape of beams in the radiative thermal transfer between a periodic array of such beams and a substrate. In this method, rigorous coupled wave analysis (RCWA) calculations are needed in order to calculate the Green's functions based on modified Sipe's formalism [30,31]. The RCWA formalism offers significant flexibility for the investigation of arbitrarily shaped structures, and the accuracy of the final results can easily be determined based on a convergence test in which the number of spatial harmonics is increased. This method boosts the numerical efficiency compared to similar calculations based on the finite-difference time-domain (FDTD) method [32]. For this paper, we have implemented a stable version of the RCWA technique [33,34] with a highly improved convergence rate [35]. In this version, in addition to harmonics of the permittivities of stacked layers, harmonics of the inverse of them are also used in the calculations [35,36]. This modification is very important since in this way usually a much smaller number of harmonics is needed to reach the convergence which saves a huge amount of computational time.

The thermal transfer between two gratings patterned in semi-infinite substrates has been investigated using the scattering method [14,37–40]. The scattering trace formulas have also been incorporated for structures made of two or even multiple bodies [41–43]. Here, we consider the thermal transfer between a periodic array of finite-sized beams with three different beam shapes and a planar substrate in a wide range of distances from the far-field to near-field regime. Moreover, for comparison purposes we have investigated the results of approximation methods such as the modified proximity approximation [25–27,44] and far-field approximation [27] that have been developed for thermal transfer calculations. The proximity approximation used here is called modified in the sense that it does consider the finite thickness of the beams and neglects part of the thermal transfer that transmits through the beams.

In this paper, we consider periodic arrays of silicon carbide (SiC) beams with rectangular, ellipsoidal, and triangular

*chalabi@stanford.edu
†mehasman@technion.ac.il
‡brongersma@stanford.edu

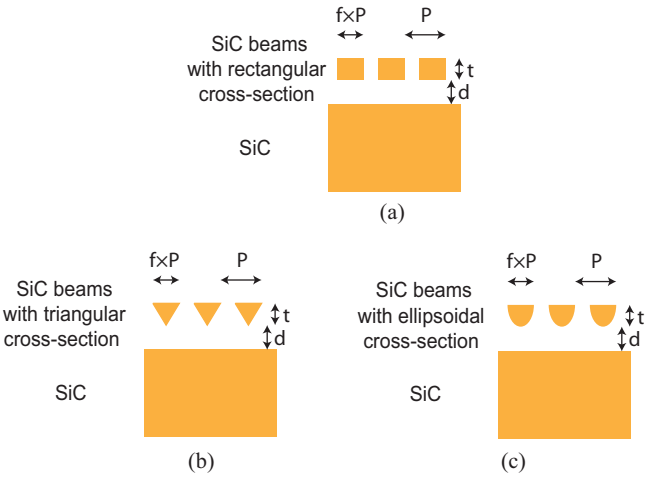

FIG. 1. (Color online) SiC beams with (a) rectangular, (b) triangular, and (c) ellipsoidal cross-sections are placed in front of a SiC substrate. The thickness of the beams is shown by t, and the spacing between the beams and the substrate is denoted by d. The top width of each beam is taken to be equal to the product of the width fraction and array period fP. The distances involved for these structures are defined in the figure.

cross-sections placed above a continuous slab of SiC (see Fig. 1). Silicon carbide is a polar semiconductor that supports a strong phononic resonance at a wavelength around 10 μm. At this wavelength, the permittivity swings from positive to negative values. On the long wavelength side, the permittivity is very large and positive, and optical Mie resonances in the beams can enhance the thermal transfer over planar structures [27]. On the other hand, at wavelengths where the permittivity becomes negative the surface can support surface phonon polariton (SPhP) excitations which are electromagnetic waves coupled to collective lattice vibrations. These surface waves can provide a significant boost in the thermal transfer in the near-field regime.

Using our developed formalism [27], the thermal conductance between the SiC beams and the slab of SiC is numerically evaluated. The details of the notations used for the geometrical parameters involved are shown in Fig. 1. The variation in thermal conductance with the width fraction of beams is explored for different array periodicities. Specifically, we have considered two different periodicities of $P = 0.1$ μm and $P = 10$ μm, and the thickness of the beams in the considered structures is taken to be $t = 0.5$ μm.

Based on Refs. [45,46], it is assumed that the relative permittivity of SiC can be written as $\epsilon = \epsilon_\infty + \omega_0^2(\epsilon_s - \epsilon_\infty)(\omega_0^2 - \omega^2 + i\omega\delta)^{-1}$, with $\epsilon_\infty = 6.7$, $\epsilon_s = 10$, $\delta/\omega_0 = 0.006$, and $\omega_0/(2\pi) = 2.38 \times 10^{13}$ sec^{-1}(12.6 μm). In addition, the temperature that is assumed in the numerical calculations is $T = 315$ K.

II. NUMERICAL IMPLEMENTATION

As was discussed in Ref. [27], computation of the thermal transfer at each frequency involves a two-dimensional integration over the k_x, k_y plane. Corresponding to each point in the k_x, k_y plane, an RCWA calculation should be carried out. We know that if we incorporate n harmonics and our structure is decomposed into L vertical layers, then each of the RCWA calculations will need a computational time proportional to n^3L. This fact makes the computational time much longer for the ellipsoidal and triangular beams as compared to the rectangular beams. In addition to the increased number of layers, having abrupt changes in thermal transfer requires us to incorporate more harmonics. For the current paper, we have used the VEGAS method for integration over the k_x, k_y plane which is based on Monte Carlo important sampling of the integrand function [47]. This method tries to minimize the number of function calls and is identified as a fast integration technique to maximize the speed of calculations.

We found that we needed to decompose the triangular and ellipsoidal shaped beams into 100 layers to reach convergence. The use of such a large number of layers will increase the computational time proportionally. In order to do required calculations in a decent amount of time, we ran our simulation codes on a computer cluster using MPI [48] for parallelization. Specifically, we used 40 nodes where each node is equipped with Intel Westmere-EP processors (24 cores per node). We also capitalized on the mirror symmetries present in our studied structures to save time [49]. Moreover, because of the rapid variations of thermal transfer across the period, especially for large periods and for the case of triangular shaped beams, we had to employ 81 harmonics in the RCWA-based simulations in order to reach convergence with less than 5% error.

III. NUMERICAL RESULTS

At small periodicities ($P = 0.1$ μm), the thermal conductance changes negligibly across the period, and this is the case for three different beam shapes considered. This is because of the fact that effective medium theories [19–24] become accurate at these small periodicities. Note that this does not hold regarding the part of the thermal transfer that radiates from the substrate and transmits through the array beams. In fact this part of thermal transfer will not become uniform across the period no matter how small the periodicity is chosen as a result of discontinuity of the permittivity across the period in this plane. However, the magnitude of this part becomes negligible compared with the total thermal radiation that enters the array in the near-field regime. Therefore, even using just one harmonic in the regime of small periodicity (compared with the surface phonon polariton resonance wavelength) will lead to relatively accurate results.

On the contrary, this is not the case for large periodicities. Figure 2 shows the contribution to the total thermal conductance at different spatial locations x across the period. The contributions are calculated in the plane right above the substrate for different beam shapes. The width fraction is assumed to be the same value of 0.4 in all cases and the periodicity is assumed to be equal to 10 μm. Note that since we have translational symmetry in the y direction, the contributions to the thermal conductance do not vary along that direction. Figure 2(a) shows the results when the beams are spaced 1 μm from the substrate. This figure shows that variations are quite smooth for this spacing. By decreasing the distance further to 0.1 μm and reaching the near-field regime, more abrupt changes can be observed in the contributions to

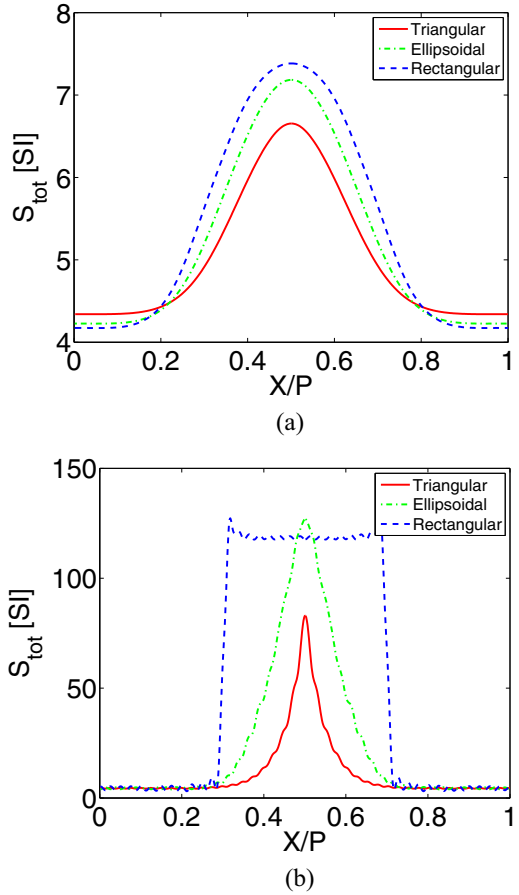

FIG. 2. (Color online) Contributions to the thermal conductance for the structure shown in Fig. 1 across a period for different beam shapes, by assuming a constant value of $f = 0.4$ and periodicity of $P = 10$ μm, when they are separated by (a) $d = 1$ μm and (b) $d = 0.1$ μm.

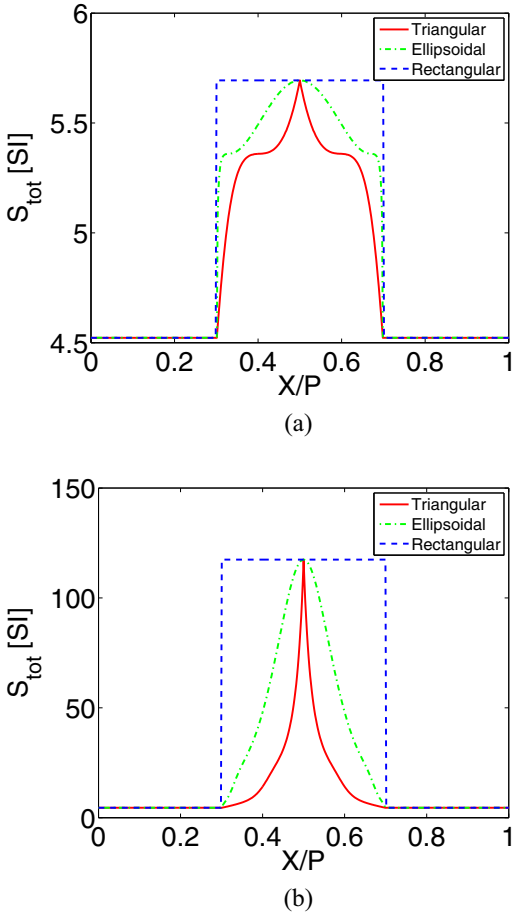

FIG. 3. (Color online) The results of modified proximity approximation for variation of the thermal conductance across a period for different beam shapes, by assuming a constant value of $f = 0.4$, when they are separated by (a) $d = 1$ μm and (b) $d = 0.1$ μm. The contributions to the total thermal transfer are calculated in the plane right above the substrate for different beam shapes.

the total thermal conductance across the period [see Fig. 2(b)]. Having such abrupt changes, especially in the case of triangular shaped beams, 81 harmonics were needed for reaching the convergence.

The results of proximity approximation are shown for comparison in Fig. 3. This figure shows that there exists good agreement with the exact results in the limit of small separation [cf. Fig. 2(b) and Fig. 3(b)]. Note that these plots show the total thermal conductance from the substrate to both the beams and the space that lies beyond the beams.

The results of the calculations for the structure shown in Fig. 1 with different values of periodicity and width fractions are shown in Fig. 4 for the case of $d = 100$ μm. The total thermal conductance for the small periodicity ($P = 0.1$ μm) is monotonically increasing with increasing width fraction. This comes from the fact that gratings with higher width fractions feature more SiC material that is located near the adjacent SiC substrate. This then naturally facilitates higher evanescent coupling. However, for the larger periodicity ($P = 10$ μm), a peak is achieved in thermal transfer for all three beam shapes at a width fraction that is neither 0 nor 1. Noting that the phononic resonance wavelength of the SiC is around 10 μm, this fact can be attributed to the possibility to excite extra Mie resonances supported by the beams in the structures with large periodicity. For comparison purposes, the thermal conductance is also calculated based on the far-field approximation (FFA) [27]. As we expect, this approximation gives a lower value than the exact calculation because it neglects contributions to the thermal transfer arising from multiple reflections of the thermal radiation [27]. However, the trend in the variation of the thermal energy flux with width fraction is qualitatively similar for all three beam shapes considered for both periodicities of $P = 0.1$ μm and $P = 10$ μm.

Mie resonances can be identified as sharp peaks in the spectral contributions to the thermal energy flux [27]. Such resonances can enhance the thermal transfer and give rise to the highest value of the thermal conductance for a nonunity width fraction. In Fig. 5, the thermal conductance frequency spectrum is shown for different beam shapes with the width fraction of 0.7 and for both periodicities of $P = 0.1$ μm and $P = 10$ μm. This figure clearly shows how the resonant channels cause the thermal conductance to be higher in the case of larger periodicity.

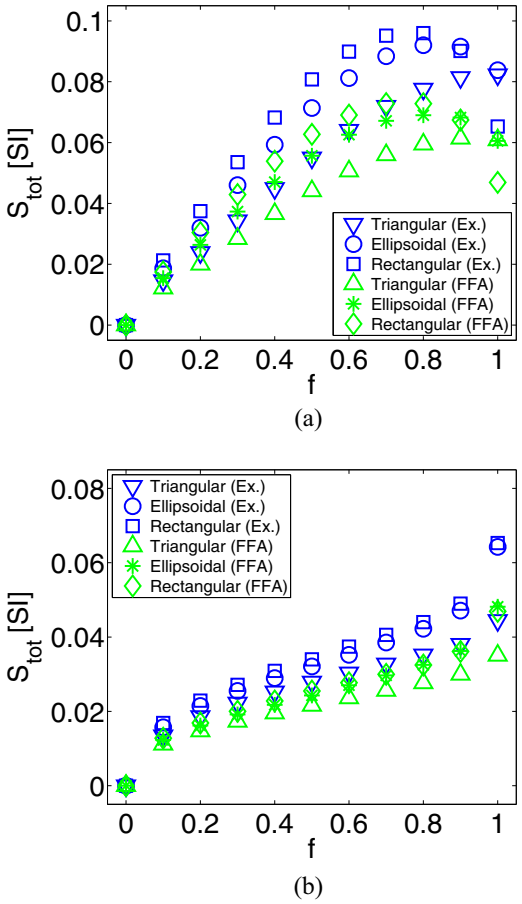

FIG. 4. (Color online) Variation of total thermal conductance vs width fraction for the structures shown in Fig. 1, with the periodicity of (a) $P = 10\ \mu$m and (b) $P = 0.1\ \mu$m. Both the exact results when the separation is $d = 100\ \mu$m as well as the results based on FFA are shown.

By decreasing the spacing between the array and substrate to $d = 0.25\ \mu$m, the thermal conductance for different width fractions and periodicities increases (see Fig. 6). However, in this regime the thermal conductance monotonically increases with increasing width fraction. Note that the dependence is not necessarily linear with increasing width fraction. However, this increase becomes more linear for large values of the periodicity. A similar linear variation with the width fraction has recently been reported for the near-field thermal transfer between the polar gratings [50]. This is consistent with our intuition that for large values of the periodicity the interactions between neighboring beams are negligible and that the modified proximity approximation becomes more accurate (see Appendix A). On the other hand, in the regime of small periodicities the thermal transfer does not feature a linear relationship with width fraction especially for the rectangular shaped beams (see rectangular subsection from Appendix B). However, for the triangular and ellipsoidal beams, the variation becomes more linear with width fraction even in the low periodicity regime (see triangular and ellipsoidal subsections from Appendix B).

Figure 7 shows the dependence of the thermal conductance on the spacing between the array and substrate for different

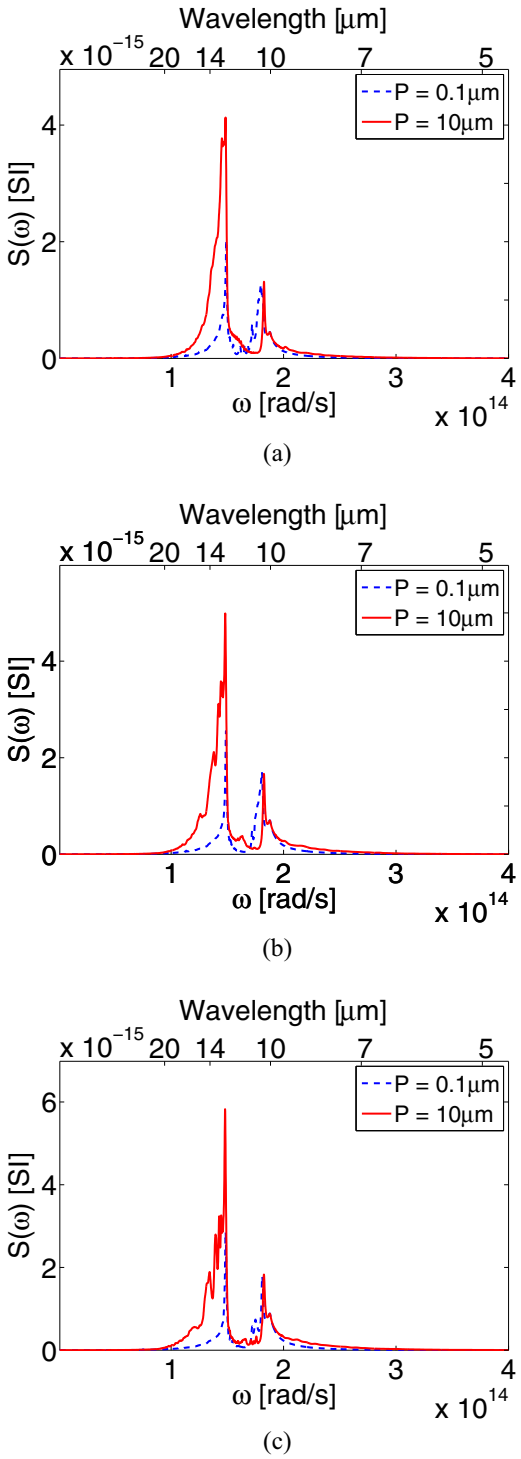

FIG. 5. (Color online) Thermal conductance frequency spectrum for the array of beams with (a) triangular, (b) ellipsoidal, and (c) rectangular cross-sections for two periodicities of $P = 10\ \mu$m and $P = 0.1\ \mu$m. The width fraction is assumed as 0.7, and the separation is $d = 100\ \mu$m.

beam shapes and for periodicities of $P = 10\ \mu$m and $P = 0.1\ \mu$m. From the figure it is clear that the far-field thermal transfer is higher for the arrays with larger periodicity ($P = 10\ \mu$m) for all three geometries that were considered. This can again be attributed to the presence of extra Mie

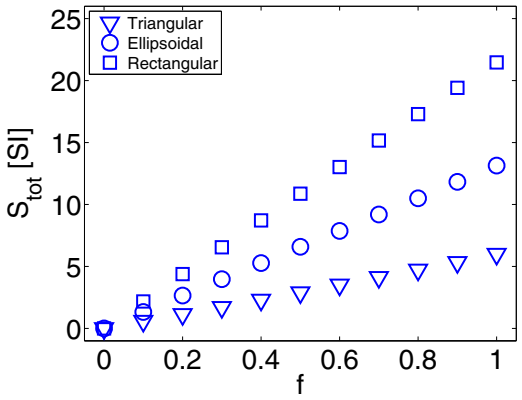

FIG. 6. (Color online) Variation of total thermal conductance vs width fraction for the structures shown in Fig. 1, with the periodicity of (a) $P = 10\ \mu$m and (b) $P = 0.1\ \mu$m. Results are shown when the separation is $d = 0.25\ \mu$m.

resonances in the periodic structure with larger periodicity. For both the triangular and ellipsoidal shaped beams, this will remain the case for very small distances as well. However, the thermal transfer for the array of rectangular shaped beams with smaller periodicity ($P = 0.1\ \mu$m) remains the same and is even higher compared with the one with larger periodicity ($P = 10\ \mu$m). Additional calculations show that a further reduction in the array period will lead to a decrease in the thermal transfer for the rectangular beams as well. These results show that we will experience rapid reduction in thermal transfer for ellipsoidal and triangular shaped beams by decreasing the periodicity in clear contrast with the array of rectangular shaped beams.

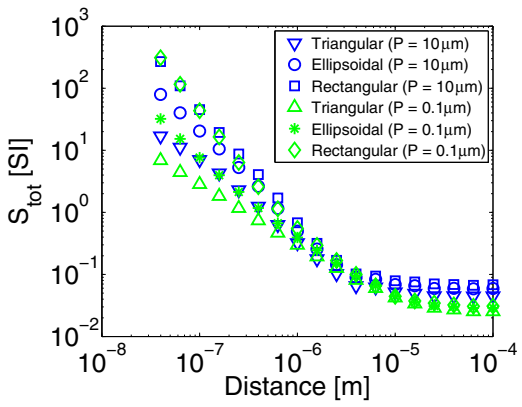

FIG. 7. (Color online) Variation of the total thermal conductance as a function of distance for the structures shown in Fig. 1 with $f = 0.4$ and $d_{\text{beam}} = 0.5\ \mu$m. Calculations are done for two periodicities of $P = 0.1\ \mu$m and $P = 10\ \mu$m.

Aside from the magnitude of the thermal conductance, it is of great interest to analyze the shape-dependent variation of the thermal conductance with the array-to-substrate spacing d. In the near-field, the thermal conductance varies as d^{-2} for the case of rectangular shaped beams. From Fig. 7, it is clear that this fact holds irrespective of the periodicity. Moreover, a similar fact holds for triangular and ellipsoidal shaped beams in which the near-field thermal transfer varies as d^{-1} and $d^{-3/2}$, respectively.

It is shown that for the case of two semi-infinite slabs that are made of materials that support coupled surface modes (CSM), the density of states (DOS) is proportional to d^{-2} in the near-field regime [51]. This will lead to a similar variation in the near-field thermal transfer versus spacing between the slabs. In the limit of large periodicity, the variation of the spacing across the period for different beam shapes considered can be assumed as adiabatic changes. Based on this fact and by using the proximity approximation, it is shown in appendix A why the above-mentioned simple scaling laws hold for the near-field thermal transfer. On the other hand, by exploration of the limit of small periodicities, we have shown in Appendix B why the same power laws hold in the low periodicity regime for the three different beam shapes considered.

IV. CONCLUSIONS

In this paper, we have investigated the variation of thermal transfer for three different periodic beam shapes. Using the technique developed previously which is based on RCWA, we obtained the thermal conductance between a slab of SiC and an array of SiC beams of rectangular, triangular, and ellipsoidal cross-section. The obtained results show that near-field thermal conductance in the limit of large periodicity varies with d^{-2}, $d^{-3/2}$, and d^{-1} with distance, respectively for rectangular, ellipsoidal, and triangular cross-section. Moreover, results show that near-field thermal transfer changes linearly with width fraction in these cases. In the limit of small periodicity, even though the scaling law remains nearly the same, the thermal transfer decreases rapidly especially for the case of triangular and ellipsoidal cross-section. In addition, the thermal transfer will not linearly scale with width fraction anymore, particularly for the case of rectangular shaped beams. On the other hand, in the far-field regime we can easily see that using arrays with larger periodicities but with the same width fraction show increased thermal transfer. This is attributed to the extra Mie resonances that these structures support when they have a large periodicity.

The obtained numerical results are checked with analytical solutions in both regimes of large and small periodicities, where proximity approximation or effective medium theories become increasingly accurate, respectively. Moreover, the far-field thermal transfer behavior for different cross-sections is

compared with far-field approximation technique. The results of this paper can be directly applied for designing devices which work based on near-field thermal transfer.

ACKNOWLEDGMENTS

The authors greatly acknowledge support from the DOE 'Light-Material Interactions in Energy Conversion' Energy Frontier Research Center under Grant DE-SC0001293. The authors also would like to thank Emanuele Francesco Pecora for helpful discussions.

APPENDICES

In the following appendices, we analytically investigate the distance variation of thermal conductance in regimes of large and small periodicities. We know that in the limit of large periodicity, proximity approximation becomes accurate. On the other hand, in the regime of very small periodicity compared to the dominant resonance wavelength of the material, the use of effective medium theories becomes viable.

APPENDIX A: THERMAL CONDUCTANCE IN THE LIMIT OF LARGE PERIODICITY

The near-field thermal transfer between two semi-infinite slabs will vary as $S(z) = \alpha z^{-2}$ with the separation z. This is the case for the structures that are made of materials such as SiC that support coupled surface modes (CSM) [51]. Using this fact and based on the proximity approximation, near-field thermal transfer can be calculated for different beam shapes in the limit of large periodicity.

By considering only a single period, a representative beam is assumed to extend from $x = -fP/2$ to $x = fP/2$ and to have a thickness of t. Moreover, the smallest separation of the beam from the substrate is assumed to be d.

For rectangular shaped beams, in which $z = d$, we have

$$\begin{aligned} S &= \frac{2}{P}\int_0^{fP/2} \frac{\alpha}{z^2} dx \\ &= f\alpha d^{-2}, \end{aligned} \tag{A1}$$

verifying the fact that near-field thermal transfer varies as d^{-2} for the rectangular shaped beams.

For triangular shaped beams, in which $z = d + \frac{2tx}{fP}$, we have

$$\begin{aligned} S &= \frac{2}{P}\int_0^{fP/2} \frac{\alpha}{z^2} dx \\ &= \frac{f\alpha}{t}\int_d^{d+t} \frac{dz}{z^2} \\ &\cong f\alpha t^{-1} d^{-1}, \end{aligned} \tag{A2}$$

verifying the fact that near-field thermal transfer varies as d^{-1} for the triangular shaped beams.

For ellipsoidal shaped beams, in which $z = d + t(1 - \sqrt{1 - \frac{4x^2}{f^2P^2}})$, we have

$$\begin{aligned} S &= \frac{2}{P}\int_0^{fP/2} \frac{\alpha}{z^2} dx \\ &= \frac{f\alpha}{d\,(d+2t)} + \frac{2f\alpha t}{d^{3/2}\,(d+2t)^{3/2}} \arctan\left(\sqrt{\frac{2t+d}{d}}\right) \\ &\cong \frac{f\alpha}{2dt} + \frac{\pi f\alpha t}{d^{3/2}\,(2t)^{3/2}} \cong \frac{\pi f\alpha}{2\sqrt{2}} t^{-1/2} d^{-3/2}, \end{aligned} \tag{A3}$$

verifying the fact that near-field thermal transfer varies as $d^{-3/2}$ for ellipsoidal shaped beams.

We know that the assumption of $S(z) = \alpha z^{-2}$ is only valid when the thickness of the structure is much larger than the distance z [29]. Because of that, it may be argued that this assumption does not hold for z values nearly equal or larger than the thickness of the structure at that point. This fact can be addressed by changing the upper bound of the integral from $z = d + t$ to a smaller value. However, the new bound will be a fraction of thickness t. This causes the final result regarding the power law to remain unchanged.

APPENDIX B: THERMAL CONDUCTANCE IN THE LIMIT OF SMALL PERIODICITY

For sufficiently small periodicities, we know that a structure with a periodically varying permittivity can be modeled as a homogenous material with appropriate effective permittivities. In the following, we show the material permittivity of the array with $\epsilon_{M,A}$ and the one for the substrate with ϵ_S. In the regime of very low periodicity, we can decompose the array structure into layers with different effective permittivities. Taking the fractional width of the beam material for the layer at height z to be equal to $f(z)$, this layer has effective permittivities of $\epsilon_{\text{eff},\parallel} = 1 + f(z)(\epsilon_{M,A} - 1)$ and $\epsilon_{\text{eff},\perp} = (1 + f(z)(\epsilon_{M,A}^{-1} - 1))^{-1}$.

Treating these layers as anisotropic material will lead to mixing of the s and p polarization. For simplification, we will model them as isotropic material with $\epsilon_{\text{eff}} = 1 + f(z)(\epsilon_{M,A} - 1)$ in our analysis. The results obtained from this approximation may be a bit off from the exact ones. However, the emphasis here is on the study of the scaling behavior with the separation. For such a study, we expect the vertical variation of the filling fraction of array material for the representation of each shape to be the most important factor. Using this approximation, we can view the structure as a 1D structure but with a graded index. We know that the thermal transfer for such a 1D structure can be calculated based on the following [29]:

$$S = \int_0^\infty \int_0^\infty \frac{\epsilon_0 V \omega \Im(\epsilon_S)}{-\pi^2} (\theta(\omega, T_1) - \theta(\omega, T_2))\, \beta d\beta d\omega, \tag{B1}$$

where V is given by

$$V = \frac{-\omega\mu_0}{8\Im(k_z)|k_z|^2}\Re\Big\{[k_z(1-R_s)(1+R_s^*)-k_{zv}|T_s|^2] + \frac{\beta^2+|k_z|^2}{\epsilon_S k_0^2}[k_z(1-R_p)(1+R_p^*)-k_{zv}|T_p|^2]\Big\} \quad \text{(B2)}$$

in which $R_{p,s}$ and $T_{p,s}$ are the reflection and transmission coefficients corresponding to p and s polarized waves, and $\theta(\omega,T) = \hbar\omega/(exp(\hbar\omega/k_BT)-1)$ is the mean energy of a harmonic oscillator with angular frequency of ω at temperature T. Moreover, β corresponds to the transverse component of the wave vector. Finally, $k_z = \sqrt{\epsilon_S\omega^2/c^2-\beta^2}$ and $k_{zv} = \sqrt{\omega^2/c^2-\beta^2}$ are z components of the wave vector in the substrate and vacuum, respectively.

In the limit of large β, the contribution from s polarization becomes negligible, and this expression reduces to

$$V = \frac{-\omega\mu_0}{4k_0^2|\epsilon_S|^2}\Im\{\epsilon_S(1+R_p)(1-R_p^*)\}. \quad \text{(B3)}$$

Calculation of the reflection coefficient is done through the following analysis. We know that we can define an effective matrix M for any planar structure [52], where the reflection coefficient can be expressed in terms of its elements. This matrix for the case of a planar structure composed of an air gap and the array with its own M_A matrix can be written as

$$M = \begin{bmatrix} \cosh(\beta d) & \frac{k_0}{\beta}\sinh(\beta d) \\ \frac{\beta}{k_0}\sinh(\beta d) & \cosh(\beta d)\end{bmatrix}\begin{bmatrix} m_{A,11} & m_{A,12} \\ m_{A,21} & m_{A,22}\end{bmatrix} = \begin{bmatrix} m_{11} & m_{12} \\ m_{21} & m_{22}\end{bmatrix}. \quad \text{(B4)}$$

In terms of M matrix elements, R_p can be written as

$$R_p = \frac{m_{11}+\frac{\beta m_{12}}{k_0}-\epsilon_S m_{22}-\epsilon_S\frac{k_0 m_{21}}{\beta}}{m_{11}+\frac{\beta m_{12}}{k_0}+\epsilon_S m_{22}+\epsilon_S\frac{k_0 m_{21}}{\beta}} \quad \text{(B5)}$$

such that

$$\epsilon_S(1+R_p)(1-R_p^*) = \frac{4|\epsilon_S|^2\left(m_{11}+\frac{\beta m_{12}}{k_0}\right)\left(m_{22}+\frac{k_0 m_{21}}{\beta}\right)^*}{\left|m_{11}+\frac{\beta m_{12}}{k_0}+\epsilon_S m_{22}+\epsilon_S\frac{k_0 m_{21}}{\beta}\right|^2}. \quad \text{(B6)}$$

Therefore, we will have

$$V = \frac{\omega\mu_0}{k_0^2}\left|m_{11}+\frac{\beta m_{12}}{k_0}+\epsilon_S m_{22}+\epsilon_S\frac{k_0 m_{21}}{\beta}\right|^{-2} \times \Im\left\{\left(m_{11}+\frac{\beta m_{12}}{k_0}\right)^*\left(m_{22}+\frac{k_0 m_{21}}{\beta}\right)\right\}. \quad \text{(B7)}$$

If we substitute the elements of matrix M from Eq. (B4), after some simplifications, we will get the following:

$$V = \frac{\omega\mu_0}{k_0^2}|\cosh(\beta d)+\epsilon_S\sinh(\beta d)|^{-2}\,\Im(g_m) \times\left|1+g_m\frac{\sinh(\beta d)+\epsilon_S\cosh(\beta d)}{\cosh(\beta d)+\epsilon_S\sinh(\beta d)}\right|^{-2}, \quad \text{(B8)}$$

where parameter g_m is defined in terms of M_A matrix elements as

$$g_m \doteq \frac{m_{A,22}+\frac{k_0 m_{A,21}}{\beta}}{m_{A,11}+\frac{\beta m_{A,12}}{k_0}}. \quad \text{(B9)}$$

Now it remains to calculate the M_A matrix for the graded index material.

Elements of matrix M_A corresponding to the graded index material should satisfy the following equations:

$$\begin{aligned}\frac{dm_{A,12}}{dz} &= \epsilon_A k_0 m_{A,11}\\ \frac{dm_{A,21}}{dz} &= \frac{\beta^2}{\epsilon_A k_0}m_{A,22}\\ \frac{dm_{A,22}}{dz} &= \epsilon_A k_0 m_{A,21}\\ \frac{dm_{A,11}}{dz} &= \frac{\beta^2}{\epsilon_A k_0}m_{A,12}\end{aligned} \quad \text{(B10)}$$

with the following initial conditions:

$$\begin{aligned}m_{A,11}(0) &= m_{A,22}(0) = 1\\ m_{A,12}(0) &= m_{A,21}(0) = 0\end{aligned} \quad \text{(B11)}$$

Note that the determinant of the M_A matrix $D = m_{A,11}m_{A,22} - m_{A,12}m_{A,21}$ remains constant and equal to one as a function of z.

1. Rectangular beams

If the array of beams has a width fraction of f, then $\epsilon_A = 1+(\epsilon_{M,A}-1)f$. In this case, the permittivity is not changing with height, and the M_A matrix is given by

$$M_A = \begin{bmatrix} \cosh(\beta t) & \frac{\epsilon_A k_0}{\beta}\sinh(\beta t) \\ \frac{\beta}{\epsilon_A k_0}\sinh(\beta t) & \cosh(\beta t)\end{bmatrix}. \quad \text{(B12)}$$

Therefore, g_m is equal to

$$g_m = \frac{\cosh(\beta t)+\epsilon_A^{-1}\sinh(\beta t)}{\cosh(\beta t)+\epsilon_A\sinh(\beta t)}. \quad \text{(B13)}$$

Plugging the above expression for g_m into Eq. (B8), we arrive at

$$\frac{-\epsilon_0\omega}{\pi^2}V\Im(\epsilon_S) = \frac{4}{\pi^2}\Im(\gamma_S)\Im(\gamma_A)e^{-2\beta d}(1-e^{-2\beta t}) \times|(1+\gamma_A e^{-2\beta t})(1+\gamma_S e^{-2\beta d})(1-\gamma_A) + (1-\gamma_A e^{-2\beta t})(1-\gamma_S e^{-2\beta d})(1+\gamma_A)|^{-2} \quad \text{(B14)}$$

where

$$\begin{aligned}\gamma_A &= \frac{1-\epsilon_A}{1+\epsilon_A}\\ \gamma_S &= \frac{1-\epsilon_S}{1+\epsilon_S}.\end{aligned} \quad \text{(B15)}$$

This is the generalized expression for the Swihart geometry [29] for the case where the slab and substrate are of different materials.

In the limit of large thickness, we have

$$\frac{-\epsilon_0\omega}{\pi^2}V\Im(\epsilon_S)=\frac{1}{\pi^2}\frac{\Im(\gamma_S)\Im(\gamma_A)e^{-2\beta d}}{|1-\gamma_S\gamma_A e^{-2\beta d}|^{-2}}. \tag{B16}$$

By substitution of this expression into Eq. (B1), it can be easily checked that the near-field thermal transfer will obey the d^{-2} law, as was discussed for the case of the Swihart geometry [29].

2. Triangular beams

For the case of triangular shaped beams, if we assume the thickness to be t, then the width fraction varies linearly with height z as $f(z)=fzt^{-1}$. Therefore, the permittivity varies as

$$\epsilon_A(z)=1+(\epsilon_{M,A}-1)f(z)=1+\zeta^{-1}t^{-1}z, \tag{B17}$$

where the parameter $\zeta\doteq f^{-1}(\epsilon_{M,A}-1)^{-1}$ is defined for later use.

Using the above expression for permittivity, M_A matrix elements can be determined based on Eqs. (B10) and (B11). Following the conventional procedure for solving these equations [53], these elements can be expressed in terms of Whittaker functions. However, we are only interested in the parameter g_m for thermal transfer calculation. After simplifications this parameter can be expressed in terms of the modified Bessel functions as

$$g_m=\frac{K_0(\zeta\beta t)-I_0(\zeta\beta t)\Gamma(\zeta,\beta t)}{K_1(\zeta\beta t)+I_1(\zeta\beta t)\Gamma(\zeta,\beta t)} \tag{B18}$$

where

$$\Gamma(\zeta,\beta t)=\frac{K_0((\zeta+1)\beta t)-(1+\zeta^{-1})K_1((\zeta+1)\beta t)}{I_0((\zeta+1)\beta t)+(1+\zeta^{-1})I_1((\zeta+1)\beta t)}. \tag{B19}$$

In the limit of large thickness $\beta t\gg 1$, we have

$$g_m=1+f\frac{1-\epsilon_{M,A}}{2\beta t}+O(\beta^{-2}t^{-2}). \tag{B20}$$

Therefore, $\Im(g_m)=-f\Im(\epsilon_{M,A})/(2\beta t)$. This proves the fact that near-field thermal transfer will vary as $d^{-1}t^{-1}$, even in the regime of very low periodicity. We note that this result holds when we neglect the s and p polarization coupling, however numerical results show that the scaling behavior of thermal transfer is very similar if we include this effect and treat the problem exactly.

3. Ellipsoidal beams

In this case, the width fraction varies with height z as $f(z)=f\sqrt{1-(1-\frac{z}{t})^2}$ and permittivity can be written as $\epsilon_A(z)=1+(\epsilon_{M,A}-1)f(z)$. Similar to the previous case, the variation behavior of M_A matrix elements can be explored.

Analysis of asymptotic behavior of the parameter g_m in this case shows that for large values of thickness $\beta t\gg 1$ we have

$$g_m=1+8f\frac{1-\epsilon_{M,A}}{9\sqrt{\beta t}}+O(\beta^{-1}t^{-1}). \tag{B21}$$

Therefore, $\Im(g_m)=-8f\Im(\epsilon_{M,A})/(9\sqrt{\beta t})$. This proves the fact that near-field thermal transfer will vary as $d^{-3/2}t^{-1/2}$, even in the regime of very low periodicity. Again, we should emphasize that this result holds when we treat layers corresponding to the array of beams as isotropic material and neglect the s and p coupling. Numerical results show that the scaling behavior does not change that much by exact treatment of the problem, as in the previous case.

[1] D. Polder and M. Van Hove, Phys. Rev. B **4**, 3303 (1971).
[2] A. V. Shchegrov, K. Joulain, R. Carminati, and J.-J. Greffet, Phys. Rev. Lett. **85**, 1548 (2000).
[3] J.-P. Mulet, K. Joulain, R. Carminati, and J.-J. Greffet, Microscale Thermophys. Eng. **6**, 209 (2002).
[4] M. Planck, *The Theory of Heat Radiation (1914)* (Kessinger Publishing, LLC, 2007).
[5] N. Shitrit, I. Yulevich, E. Maguid, D. Ozeri, D. Veksler, V. Kleiner, and E. Hasman, Science **340**, 724 (2013).
[6] N. Dahan, Y. Gorodetski, K. Frischwasser, V. Kleiner, and E. Hasman, Phys. Rev. Lett. **105**, 136402 (2010).
[7] J. A. Schuller, T. Taubner, and M. L. Brongersma, Nat. Photon. **3**, 658 (2009).
[8] N. Dahan, A. Niv, G. Biener, Y. Gorodetski, V. Kleiner, and E. Hasman, Phys. Rev. B **76**, 045427 (2007).
[9] C. R. Otey, W. T. Lau, and S. Fan, Phys. Rev. Lett. **104**, 154301 (2010).
[10] P. Ben-Abdallah and S.-A. Biehs, Appl. Phys. Lett. **103**, 191907 (2013).
[11] P. Ben-Abdallah and S.-A. Biehs, Phys. Rev. Lett. **112**, 044301 (2014).
[12] M. Francoeur, M. P. Mengüç, and R. Vaillon, J. Phys. D **43**, 075501 (2010).
[13] M. Francoeur, M. P. Mengüç, and R. Vaillon, Phys. Rev. B **84**, 075436 (2011).
[14] M. Krüger, T. Emig, and M. Kardar, Phys. Rev. Lett. **106**, 210404 (2011).
[15] C. Otey and S. Fan, Phys. Rev. B **84**, 245431 (2011).
[16] A. P. McCauley, M. T. H. Reid, M. Krüger, and S. G. Johnson, Phys. Rev. B **85**, 165104 (2012).
[17] M. T. H. Reid, A. W. Rodriguez, and S. G. Johnson, Proc. IEEE **101**, 531 (2013).
[18] A. W. Rodriguez, P.-C. Hui, D. P. Woolf, S. G. Johnson, M. Loncar, and F. Capasso, Ann. Phys. **527**, 45 (2015).
[19] S.-A. Biehs, F. S. S. Rosa, and P. Ben-Abdallah, Appl. Phys. Lett. **98**, 243102 (2011).
[20] S. Basu and L. Wang, Appl. Phys. Lett. **102**, 53101 (2013).

[21] S.-A. Biehs, M. Tschikin, and P. Ben-Abdallah, Phys. Rev. Lett. **109**, 104301 (2012).
[22] S.-A. Biehs, M. Tschikin, R. Messina, and P. Ben-Abdallah, Appl. Phys. Lett. **102**, 131106 (2013).
[23] S.-A. Biehs, P. Ben-Abdallah, F. S. S. Rosa, K. Joulain, and J.-J. Greffet, Opt. Exp. **19**, A1088 (2011).
[24] X. Liu, T. Bright, and Z. Zhang, J. Heat Transfer **136**, 092703 (2014).
[25] E. Rousseau, A. Siria, G. Jourdan, S. Volz, F. Comin, J. Chevrier, and J.-J. Greffet, Nat. Photon. **3**, 514 (2009).
[26] K. Sasihithlu and A. Narayanaswamy, Phys. Rev. B **83**, 161406 (2011).
[27] H. Chalabi, E. Hasman, and M. L. Brongersma, Phys. Rev. B **91**, 014302 (2015).
[28] H. Haus and W. Huang, Proc. IEEE **79**, 1505 (1991).
[29] H. Chalabi, E. Hasman, and M. L. Brongersma, Opt. Exp. **22**, 30032 (2014).
[30] J. E. Sipe, J. Opt. Soc. Am. B **4**, 481 (1987).
[31] S. Han, Phys. Rev. B **80**, 155108 (2009).
[32] A. W. Rodriguez, O. Ilic, P. Bermel, I. Celanovic, J. D. Joannopoulos, M. Soljačić, and S. G. Johnson, Phys. Rev. Lett. **107**, 114302 (2011).
[33] M. G. Moharam, E. B. Grann, D. A. Pommet, and T. K. Gaylord, J. Opt. Soc. Am. A **12**, 1068 (1995).
[34] M. G. Moharam, D. A. Pommet, E. B. Grann, and T. K. Gaylord, J. Opt. Soc. Am. A **12**, 1077 (1995).
[35] P. Lalanne and G. M. Morris, J. Opt. Soc. Am. A **13**, 779 (1996).
[36] L. Li, J. Opt. Soc. Am. A **13**, 1870 (1996).
[37] R. Guérout, J. Lussange, F. S. S. Rosa, J.-P. Hugonin, D. A. R. Dalvit, J.-J. Greffet, A. Lambrecht, and S. Reynaud, Phys. Rev. B **85**, 180301 (2012).
[38] J. Lussange, R. Guérout, F. S. S. Rosa, J.-J. Greffet, A. Lambrecht, and S. Reynaud, Phys. Rev. B **86**, 085432 (2012).
[39] J. Lussange, R. Guérout, and A. Lambrecht, Phys. Rev. A **86**, 062502 (2012).
[40] G. Bimonte, Phys. Rev. A **80**, 042102 (2009).
[41] M. Krüger, G. Bimonte, T. Emig, and M. Kardar, Phys. Rev. B **86**, 115423 (2012).
[42] A. W. Rodriguez, M. T. H. Reid, and S. G. Johnson, Phys. Rev. B **86**, 220302 (2012).
[43] R. Messina and M. Antezza, Phys. Rev. A **89**, 052104 (2014).
[44] C. R. Otey, L. Zhu, S. Sandhu, and S. Fan, J. Quantum Spectrosc. Radiat. Transfer **132**, 3 (2014).
[45] W. Spitzer, D. Kleinman, and D. Walsh, Phys. Rev. **113**, 127 (1959).
[46] W. Spitzer, D. Kleinman, and C. Frosch, Phys. Rev. **113**, 133 (1959).
[47] G. Peter Lepage, J. Comput. Phys. **27**, 192 (1978).
[48] W. Gropp, E. Lusk, and A. Skjellum, *Using MPI: Portable Parallel Programming with the Message-Passing Interface* (MIT Press, Cambridge, MA, 1999).
[49] B. Bai and L. Li, J. Opt. A: Pure Appl. Opt. **7**, 783 (2005).
[50] X. L. Liu and Z. M. Zhang, Appl. Phys. Lett. **104**, 251911 (2014).
[51] S.-A. Biehs, E. Rousseau, and J.-J. Greffet, Phys. Rev. Lett. **105**, 234301 (2010).
[52] M. Born and E. Wolf, *Principles of Optics*, 7th ed. (Cambridge University Press, Cambridge, UK, 1999).
[53] M. Dalarsson and P. Tassin, Opt. Exp. **17**, 6747 (2009).